

# Sn-doped $\text{Li}_{1.2}\text{Mn}_{0.54}\text{Ni}_{0.13}\text{Co}_{0.13}\text{O}_2$ cathode materials for lithium-ion batteries with enhanced electrochemical performance

Lin Zhou<sup>1</sup> · Jing Liu<sup>1</sup> · Lisi Huang<sup>1</sup> · Na Jiang<sup>1</sup> · Qiaoji Zheng<sup>1</sup> · Dunmin Lin<sup>1</sup>

Received: 13 February 2017 / Revised: 9 June 2017 / Accepted: 25 June 2017 / Published online: 11 July 2017  
© Springer-Verlag GmbH Germany 2017

**Abstract** Sn-doped Li-rich layered oxides of  $\text{Li}_{1.2}\text{Mn}_{0.54-x}\text{Ni}_{0.13}\text{Co}_{0.13}\text{Sn}_x\text{O}_2$  have been synthesized via a sol-gel method, and their microstructure and electrochemical performance have been studied. The addition of  $\text{Sn}^{4+}$  ions has no distinct influence on the crystal structure of the materials. After doped with an appropriate amount of  $\text{Sn}^{4+}$ , the electrochemical performance of  $\text{Li}_{1.2}\text{Mn}_{0.54-x}\text{Ni}_{0.13}\text{Co}_{0.13}\text{Sn}_x\text{O}_2$  cathode materials is significantly enhanced. The optimal electrochemical performance is obtained at  $x = 0.01$ . The  $\text{Li}_{1.2}\text{Mn}_{0.53}\text{Ni}_{0.13}\text{Co}_{0.13}\text{Sn}_{0.01}\text{O}_2$  electrode delivers a high initial discharge capacity of  $268.9 \text{ mAh g}^{-1}$  with an initial coulombic efficiency of 76.5% and a reversible capacity of  $199.8 \text{ mAh g}^{-1}$  at 0.1 C with capacity retention of 75.2% after 100 cycles. In addition, the  $\text{Li}_{1.2}\text{Mn}_{0.53}\text{Ni}_{0.13}\text{Co}_{0.13}\text{Sn}_{0.01}\text{O}_2$  electrode exhibits the superior rate capability with discharge capacities of 239.8, 198.6, 164.4, 133.4, and  $88.8 \text{ mAh g}^{-1}$  at 0.2, 0.5, 1, 2, and 5 C, respectively, which are much higher than those of  $\text{Li}_{1.2}\text{Mn}_{0.54}\text{Ni}_{0.13}\text{Co}_{0.13}\text{O}_2$  (196.2, 153.5, 117.5, 92.7, and  $43.8 \text{ mAh g}^{-1}$  at 0.2, 0.5, 1, 2, and 5 C, respectively). The substitution of  $\text{Sn}^{4+}$  for  $\text{Mn}^{4+}$  enlarges the  $\text{Li}^+$  diffusion channels due to its larger ionic radius compared to  $\text{Mn}^{4+}$  and enhances the structural stability of Li-rich oxides, leading to the improved electrochemical performance in the Sn-doped  $\text{Li}_{1.2}\text{Mn}_{0.54}\text{Ni}_{0.13}\text{Co}_{0.13}\text{O}_2$  cathode materials.

**Keywords** Lithium-ion battery ·  $\text{Li}_{1.2}\text{Mn}_{0.54}\text{Ni}_{0.13}\text{Co}_{0.13}\text{O}_2$  ·  $\text{Sn}^{4+}$ -doping · Electrochemical properties

## Introduction

Lithium-ion batteries (LIBs) have been widely applied in various fields due to their high energy density, long cycle life, and environmental friendliness [1, 2], such as information, transportation, and military. They are expected to a large number of promotions in hybrid electric vehicles (HEVs) and electric vehicles (EVs) in recent years [3, 4]. However, most traditional cathode materials (e.g.,  $\text{LiCoO}_2$  and  $\text{LiMn}_2\text{O}_4$ ) cannot satisfy the demand of the specific energy for HEVs and EVs. Therefore, it is a challenge to develop new cathode materials with high capacity, good rate capability, and low cost for high-power LIBs.

Li-rich oxides of  $x\text{Li}_2\text{MnO}_3 \cdot (1-x)\text{LiMO}_2$  ( $0 < x < 1$ ,  $M = \text{Mn, Ni, Co, Fe, Mn}_{1/3}\text{Ni}_{1/3}\text{Co}_{1/3} \dots$ ) have been widely studied because they could be operated at high working voltages (4.6–4.8 V vs.  $\text{Li/Li}^+$ ) with satisfied safety and high specific capacity (more than  $200 \text{ mAh g}^{-1}$ ) [5–7]. Among Li-rich layered cathodes,  $\text{Li}_{1.2}\text{Mn}_{0.54}\text{Ni}_{0.13}\text{Co}_{0.13}\text{O}_2$  (equivalently  $0.5\text{Li}_2\text{MnO}_3 \cdot 0.5\text{LiMn}_{1/3}\text{Ni}_{1/3}\text{Co}_{1/3}\text{O}_2$ , or LMNC, for short) has attracted considerable attention owing to its high discharge capacity ( $\sim 250 \text{ mAh g}^{-1}$ ) and good stability [8, 9]. However, the LMNC materials suffer from several disadvantages that limit their practical application, such as large irreversible capacity loss (ICL) in the first cycle [5, 10, 11], poor rate capability [5, 12, 13], and fast capacity fading during further cycles [11, 14, 15]. The large initial ICL and fast capacity fading mainly arise from the activation reaction of  $\text{Li}_2\text{MnO}_3$  component during the first charging process. When the charging potential is above 4.5 V, oxygen is irreversibly released as the form of “ $\text{Li}_2\text{O}$ ” along with the generation of oxygen-ion vacancies

**Electronic supplementary material** The online version of this article (doi:10.1007/s10008-017-3688-y) contains supplementary material, which is available to authorized users.

✉ Dunmin Lin  
ddmd222@sicnu.edu.cn

<sup>1</sup> College of Chemistry and Materials Science, Sichuan Normal University, Chengdu 610068, China

and lithium-ion vacancies [7, 16]. At the end of the initial charging process, transition metal (TM) ions move into some of these vacancies. This causes the decrease of  $\text{Li}^+$  insertion sites during the initial discharging process and thus induces the large initial ICL [17]. In the subsequent cycles, the rearrangement of the TM ions and the removing of vacancies could be proceed, resulting in a structural instability and fast capacity fading. The inferior rate capability is related to the poor electronic conductivity and low  $\text{Li}^+$  diffusion coefficient of  $\text{Li}_2\text{MnO}_3$  component [12, 13]. Many approaches have been taken to improve the electrochemical performance of LMNC materials, including surface modification [18, 19], mild acidic treatment [20, 21], structure and morphology controlling [22, 23], and cation doping [24–26]. In these methods, the doping of simple cations has been proved to be an effective approach to improve cycle stability and rate performance. Many metal cations (e.g., Mg [27], Zn [28], Al [29], and Cr [30]) have been successfully doped into the structure of Li-rich cathode materials. The doped cations can affect the morphology and microstructure, or stabilize the crystalline structure [31]. B. Song et al. reported that the  $\text{Li}(\text{Li}_{0.19}\text{Mn}_{0.54}\text{Ni}_{0.13}\text{Co}_{0.12}\text{Ru}_{0.01})\text{O}_2$  cathode shows a high discharge capacity of  $182 \text{ mAh g}^{-1}$  at 5 C with a capacity fade of 0.06% per cycle in 700 cycles because the appropriate Ru-doping could improve the  $\text{Li}^+$  diffusion in LMNC and promote the phase transition from layered  $\text{Li}(\text{Li}_{1/3}\text{Mn}_{2/3})\text{O}_2$  to certain spinel-like phases [32]. X. Jin et al. successfully synthesized Mg-doped LMNC via a sol-gel method, and the Mg-doping can enlarge the inter-slab distance of lattices to facilitate the  $\text{Li}^+$  insertion/extraction and thus improve the cycle stability and rate performance ( $160.5 \text{ mAh g}^{-1}$  at  $1000 \text{ mA g}^{-1}$  and remains  $127.5 \text{ mAh g}^{-1}$  after 50 cycles) of cathode materials [33]. Z. He et al. found that Zr dopant could stabilize the crystal structure of Li-rich cathode and improve the  $\text{Li}^+$  diffusion, which effectively enhances the cycle stability and rate performance of LMNC [34].

$\text{Sn}^{4+}$  has been frequently explored as a dopant for cathode materials ( $\text{Li}_3\text{V}_2(\text{PO}_4)_3$  [35],  $\text{LiFePO}_4$  [36],  $\text{Li}[\text{Ni}_{1/3}\text{Co}_{1/3}\text{Mn}_{1/3}]\text{O}_2$  [37]) of LIBs.  $\text{Sn}^{4+}$  has a larger ionic radius ( $0.71 \text{ \AA}$ ) than  $\text{Mn}^{4+}$  ( $0.53 \text{ \AA}$ ), and it is electrochemically inactive during the charging-discharging process, which cannot be reduced or oxidized. The  $\text{Sn}^{4+}$  dopant can distinctly improve the electrochemical performance of cathodes by enhancing the structural stability [38]. However, to our knowledge, there has no report on the improvement in the electrochemical performance of Li-rich  $\text{Li}_{1.2}\text{Mn}_{0.54}\text{Ni}_{0.13}\text{Co}_{0.13}\text{O}_2$  cathode materials by the doping of Sn ions. In this work,  $\text{Sn}^{4+}$  ions were introduced into the crystal structure of LMNC materials to partly substitute  $\text{Mn}^{4+}$  via a sol-gel method. The effect of  $\text{Sn}^{4+}$ -doping on the structure and electrochemical properties of the  $\text{Li}_{1.2}\text{Mn}_{0.54}\text{Ni}_{0.13}\text{Co}_{0.13}\text{O}_2$  was investigated.

## Experimental

### Sample preparation and characterizations

$\text{Li}_{1.2}\text{Mn}_{0.54-x}\text{Ni}_{0.13}\text{Co}_{0.13}\text{Sn}_x\text{O}_2$  ( $x = 0, 0.005, 0.01, 0.015, \text{ and } 0.02$ ) powders were prepared via a sol-gel method, denoted as LMNC, LMNCS0.5, LMNCS1, LMNCS1.5, and LMNCS2, respectively. Stoichiometric amounts of  $\text{Mn}(\text{CH}_3\text{COO})_2 \cdot 4\text{H}_2\text{O}$  (99%),  $\text{Ni}(\text{CH}_3\text{COO})_2 \cdot 4\text{H}_2\text{O}$  (98%),  $\text{Co}(\text{CH}_3\text{COO})_2 \cdot 4\text{H}_2\text{O}$  (99.5%),  $\text{SnCl}_4 \cdot 5\text{H}_2\text{O}$  (99%),  $\text{Li}(\text{CH}_3\text{COO})_2 \cdot 2\text{H}_2\text{O}$  (99%), and  $\text{C}_6\text{H}_8\text{O}_7 \cdot \text{H}_2\text{O}$  (99.5%) were used as the raw material. A 5% excess of  $\text{Li}(\text{CH}_3\text{COO})_2 \cdot 2\text{H}_2\text{O}$  was used to compensate for the Li loss during the calcinations. All the raw materials are purchased from Sinopharm Chemical Reagent Co., Ltd. The detailed synthesis process was kept consistent with that in the previous report [39].

The crystalline structure of all the materials were characterized using X-ray diffraction (XRD) analysis with  $\text{Cu K}\alpha$  radiation (SmartLab, Rigaku, Tokyo, Japan) at a scan rate of  $1^\circ \text{ min}^{-1}$  in the  $2\theta$  range of  $10\text{--}80^\circ$ . The X-ray photoelectron spectroscopy (XPS) analysis of LMNC and LMNCS1 was taken on a PHI 5000 Versa Probe XPS instrument (Thermo ESCALAB 250XI). A field-emission scanning electron microscope (SEM, FEI-Quanta 250) equipped with energy dispersive spectrum X-ray detector (EDS) was used for the observation of the morphologies, element composition and distribution for all the materials. The microstructures of LMNC and LMNCS1 samples were observed via transmission electron microscopy (TEM, JEM2100). The element composition of LMNC and LMNCS1 samples was measured by an inductively coupled plasma emission spectrometry (ICP-AES, Optima 7000 DV, Pe).

### Electrochemical measurements

The cathodes were fabricated by coating a slurry (80% active material, 10% acetylene black, and 10% PVDF) onto the Al current collectors followed by heat treated at  $120^\circ \text{C}$  for 12 h. The area of the cathode plates was  $1.5394 \text{ cm}^2$ . The CR-2025 coin-type half-cells were made up of prepared cathode plates, lithium anodes, and Celgard 2400 separators with  $1 \text{ mol L}^{-1}$   $\text{LiPF}_6$  dissolved in EC-DMC (at a volume ratio of 1:1) as electrolyte. All the cells were assembled and sealed in an Ar-filled glove box (MB-Labstar, Germany). The galvanostatic charge and discharge tests were measured using LANHE CT-2001A instrument (Wuhan, China) between 2.0 and 4.8 V (vs.  $\text{Li/Li}^+$ ) at different rates at room temperature. The cyclic voltammograms (CV) for the cells of sample LMNC and LMNCS1 were recorded on an electrochemical station (CHI660E, Shanghai, China) at a scanning rate of  $0.1 \text{ mV s}^{-1}$  in the voltage range of 2.0–4.8 V. The values of OCV for the LMNC and LMNCS1 cells before the cyclic voltammetry experiments were 2.355 and 2.358 V,

respectively. Electrochemical impedance spectroscopy (EIS) measurements were carried out after 10 cycles at 0.2 C and monitored at the electrochemical station (CHI660E, Shanghai, China) in the frequency range of 0.01–100,000 Hz at 5 mV voltage amplitude. The EIS results were simulated by Zview2 software.

## Results and discussions

### Microstructural characterization

Figure 1 shows the XRD patterns of the LMNC and Sn-doped LMNC samples. From Fig. 1a, all the samples possess a typical hexagonal layered  $\alpha$ -NaFeO<sub>2</sub> structure of Li-rich layered oxides in space group  $R\bar{3}m$ . The XRD patterns of Sn-doped LMNC samples are almost identical with that of LMNC sample, indicating that the doping of Sn<sup>4+</sup> has no obvious effect on the crystal structure of LMNC material. The extra weak diffraction peaks between 20° and 25°, which cannot be indexed to  $R\bar{3}m$  space group, are not impurity phase and indicate the LiMn<sub>6</sub> cation arrangement in monoclinic Li<sub>2</sub>MnO<sub>3</sub> with  $C2/m$  symmetry [4, 32, 40]. The fully splitting of (006)/(012) and (118)/(110) peaks proves that all the materials are a well-layered structure [24, 25]. From Fig. 1b, the (104) and (015) peaks firstly shift to lower angle with the increasing of Sn<sup>4+</sup> (LMNCS1 and LMNCS1.5) and then move to higher angle (LMNCS2) as the amount of Sn<sup>4+</sup> further increases, implying that the unit cell firstly expands and then slightly shrinks. No impurity peaks of SnO<sub>2</sub> can be detected, illustrating that the Sn<sup>4+</sup> ions have been successfully doped into the lattices of LMNC.

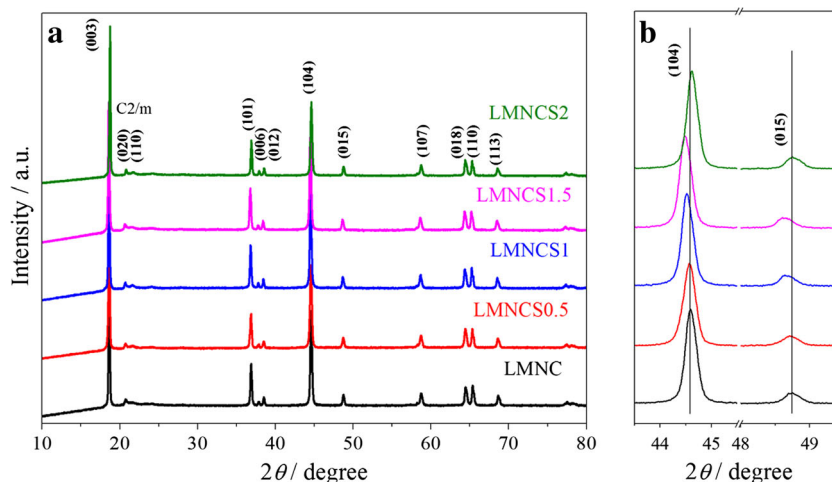
Lattice parameters of the samples were calculated by the Rietveld refinement using the  $R\bar{3}m$  hexagonal space group by the general structure analysis software (GSAS) and the results are listed in Table 1. For LMNC and LMNCS materials, Mn

**Table 1** Lattice parameters of the LMNC, LMNCS0.5, LMNCS1, LMNCS1.5, and LMNCS2 samples

Sample	<i>a</i> /Å	<i>c</i> /Å	<i>c/a</i>	<i>V</i> /Å <sup>3</sup>	<i>I</i> <sub>(003)</sub> / <i>I</i> <sub>(104)</sub>	<i>R</i> <sub>wp</sub> (%)
LMNC	2.8532	14.2421	4.9916	115.94	1.3614	6.73
LMNCS0.5	2.8540	14.2456	4.9915	116.03	1.5322	9.6
LMNCS1	2.8573	14.2586	4.9902	116.41	1.5785	6.82
LMNCS1.5	2.8592	14.2778	4.9936	116.72	1.4111	6.0
LMNCS2	2.8573	14.2586	4.9902	116.41	2.0506	7.51

(*Z* = 25), Ni (*Z* = 27), and Co (*Z* = 28) atoms have similar numbers of extranuclear electron (*Z*), which implies that these atoms have close *f<sub>j</sub>* (the scattering factor of atom *j*) and similar contribution on the intensity of diffraction peaks. Thus, it is difficult to obtain the exact atomic site occupation using XRD Rietveld refinements in the Mn-Ni-Co ternary cathode materials. It can be seen from Table 1 that the Sn<sup>4+</sup>-doping (*x* = 0.005~0.02) leads to the increasing of lattice dimensions (*a*, *c*) and the expansion of unit cell (*V*), resulting in the enlarging of Li<sup>+</sup> diffusion channels [41]. The change in lattice parameters is owing to the partly substitution of Mn<sup>4+</sup> (ionic radius = 0.53 Å) by the larger Sn<sup>4+</sup> (ionic radius = 0.71 Å). Meanwhile, compared with LMNCS1.5 sample, the values of *a*, *c*, and *V* for LMNCS2 slightly decrease. This may be due to the replacement of Sn<sup>4+</sup> for some Li<sup>+</sup>. Since Sn<sup>4+</sup> has a close ionic radius to Li<sup>+</sup> (0.76 Å), thus partly substitution of Sn<sup>4+</sup> in the Li sites is highly possible in the case of larger doping concentration of Sn<sup>4+</sup> and the Li layers doped with Sn<sup>4+</sup> ions may decrease the inter-slap spacing. Similar result has been observed in Mg-doped Li[Li<sub>0.2</sub>Ni<sub>0.13</sub>Co<sub>0.13</sub>Mn<sub>0.54</sub>]O<sub>2</sub> cathode materials [33]. There may be some electronegative lithium-ion vacancies generated to balance the electrovalence when some Sn<sup>4+</sup> substitutes for Li<sup>+</sup>. In addition, the value of *c/a* relates to the cation ordering of hexagonal structure. From Table 1, all the *c/a* values are larger than 4.899, suggesting that all the obtained samples are of well-ordered hexagonal structure

**Fig. 1** XRD patterns of LMNC and Sn-doped LMNC in the  $2\theta$  range of **a** 10–80° and **b** 43–50°



[41]. Generally, the extent of cation mixing between  $\text{Ni}^{2+}$  and  $\text{Li}^+$  in LMNC can be characterized by the value of  $I_{(003)}/I_{(104)}$  ( $R$ ) [42]. There is a serious cation mixing in Li-rich cathode materials when  $R < 1.2$ . The value of  $R$  increases from 1.3614 for the pristine LMNC to 1.5322, 1.5785, 1.4111, and 2.0506 for LMNCS0.5, LMNCS1, LMNCS1.5, and LMNCS2, respectively, indicating that the doping of  $\text{Sn}^{4+}$  can lower the extent of cation mixing. This means that the  $\text{Sn}^{4+}$ -doped LMNC may have better structural stability during further cycling [43].

The SEM images of the LMNC and Sn-doped LMNC samples are shown in Fig. 2. All the samples present a well-defined morphology with good crystallinity. From Fig. 2a, the pristine LMNC sample exhibits a homogeneous morphology with loose aggregation, which consists of sphere-like microparticles with a diameter of 100–400 nm. From Fig. 2b–d, the low contents of  $\text{Sn}^{4+}$  have no significant influence on the morphology of the LMNCS0.5, LMNCS1 and LMNCS1.5 samples. However, when the content of  $\text{Sn}^{4+}$  increases to 0.02, the LMNCS2 sample shows the morphology of rock-like grains with larger particle size. The EDS spectrum and elemental mapping images of the LMNCS1 sample are presented in Fig. 3. The EDS spectrum of LMNCS1 sample exhibits the peaks of Mn, Ni, Co, O, and Sn, indicating the presence of Sn in the LMNCS1. The elemental mapping images show that Mn, Ni, Co, and Sn are uniformly distributed in LMNCS1, which means that  $\text{Sn}^{4+}$  ions have been successfully doped into LMNC. The element composition of the LMNC and LMNCS1 samples was measured by ICP-AES. The relative element content of LMNC and LMNCS1 samples

is listed in Table 2. It is noted that the element composition of both samples are close to the target stoichiometry.

TEM, high-resolution TEM (HRTEM), and fast Fourier transform (FFT) pattern images of the LMNC and LMNCS1 samples are shown in Fig. 4. From Fig. 4a and b, the LMNC and LMNCS1 samples are made of sphere-like microparticles without any obvious difference in micromorphology. Figure 4c and d present clear parallel lattice fringes, suggesting that both samples have a good crystallinity. The interplanar distances of about 0.47 and 0.24 nm for the LMNC and LMNCS1 samples, respectively, are indexed to the (003) and (101) planes of the layered  $R\bar{3}m$  phase, respectively. These results match well with the embedded FFTs.

Figure 5 shows the XPS spectra of Co 2p, Ni 2p, Mn 2p, and Sn 3d for LMNC and LMNCS1. The observed peak positions and peak shapes of Co 2p, Ni 2p, and Mn 2p for LMNC and LMNCS1 are remarkably similar, which are also in accordance with the previous reported values [44, 45]. From Fig. 5a, the main peaks of Co 2p<sub>3/2</sub> and Co 2p<sub>1/2</sub> are at 779.9 and 794.8 eV, respectively, with a satellite peak at 789.7 eV, implying the presence of  $\text{Co}^{3+}$ . In the Ni 2p spectra (Fig. 5b), the Ni 2p<sub>3/2</sub> main peak is at 854.6 eV and the Ni 2p<sub>1/2</sub> main peak is at 872.2 eV, with two satellite peaks located at 561.0 and 578.5 eV, respectively. This proves that the main oxidation state of Ni is +2. In Fig. 5c, the 2p<sub>3/2</sub> and 2p<sub>1/2</sub> main peaks for Mn located at 642.1 and 653.8 eV, respectively, are corresponding to the existence of  $\text{Mn}^{4+}$  in the LMNC and LMNCS1 samples. For the LMNCS1 sample, the major peaks of Sn 3d<sub>5/2</sub> and Sn 3d<sub>3/2</sub> are at 486.1 and 494.4 eV (Fig. 5d), respectively, indicating that the valance of Sn in LMNCS1 is +4 [38].

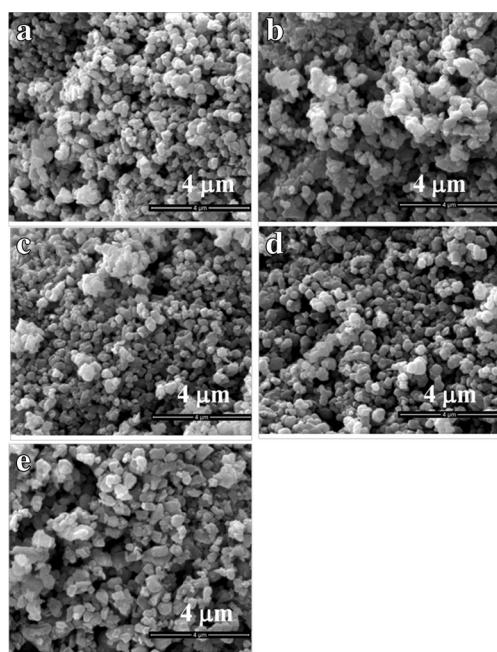
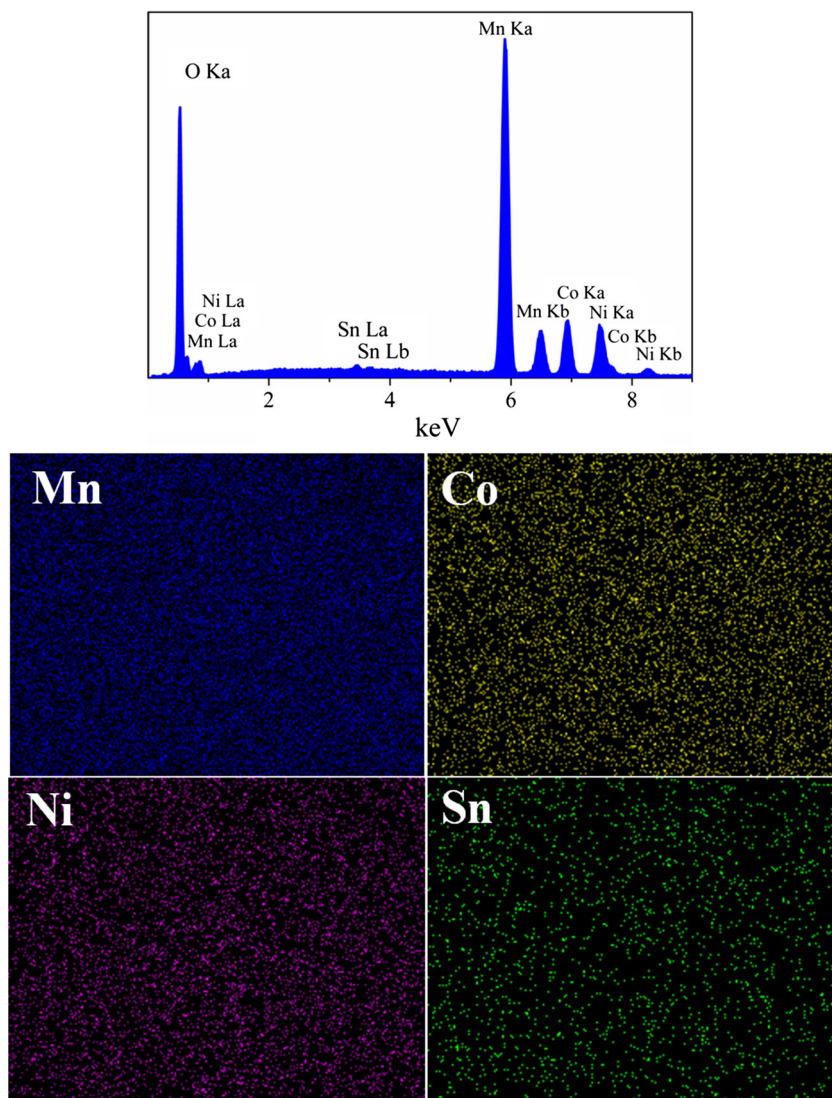


**Fig. 2** SEM images of the LMNC and Sn-doped LMNC samples: **a** LMNC, **b** LMNCS0.5, **c** LMNCS1, **d** LMNCS1.5, and **e** LMNCS2

## Electrochemical performance

The initial charge/discharge curves of the LMNC and LMNCS electrodes at 0.1 C between 2.0 and 4.8 V are shown in Fig. 6a. It can be clearly observed from Fig. 6a that all the initial charge curves have two voltage plateaus. The first one (~4.0 V) is related to the extraction of  $\text{Li}^+$  from  $\text{LiNi}_{0.33}\text{Co}_{0.33}\text{Mn}_{0.33}\text{O}_2$  structure accompanied with the oxidation of TM ions ( $\text{Ni}^{2+}/\text{Co}^{3+} \rightarrow \text{Ni}^{4+}/\text{Co}^{4+}$ ) and another one at 4.5 V is connected with the irreversibly removal of  $\text{Li}_2\text{O}$  from  $\text{Li}_2\text{MnO}_3$ , leading to the formation of  $[\text{MnO}_2]$  and the corresponding electrochemical activity [6, 7, 16, 17, 46]. The discharge profiles of LMNCS0.5 and LMNCS1 lie above that of LMNC, implying the low-level doping can elevate the discharge voltage plateau [47]. This is attributed to the increased  $\text{Li}^+$  ion diffusion caused by a small doping amount of  $\text{Sn}^{4+}$  [47, 48]. The fast  $\text{Li}^+$  ion diffusion is beneficial to the decrease of electrochemical polarization, resulting in the elevation of discharge voltage plateau for LMNCS0.5 and LMNCS1. The pristine LMNC electrode delivers the charge/discharge capacity of 337.3/251.6  $\text{mAh g}^{-1}$  in the first cycle with an initial coulombic efficiency of 74.59%.

**Fig. 3** EDS spectrum and elemental mapping images of LMNCS1



After doped with  $\text{Sn}^{4+}$ , the initial charge/discharge capacities of the LMNCS0.5, LMNCS1, LMNCS1.5, and LMNCS2 electrodes are 340.2/252.1, 351.5/268.9, 307.9/195.1, and 305.1/193.1  $\text{mAh g}^{-1}$ , with initial coulombic efficiencies of 74.1, 76.5, 63.36, and 63.29%, respectively. The ICL values for all electrodes are larger than  $80 \text{ mAh g}^{-1}$ , which are ascribed to the side reactions of electrolyte at high operating voltages and the decrease of oxygen-ion vacancies and  $\text{Li}^+$  insertion sites [47]. It is obviously noted that LMNCS1 exhibits the enhanced initial discharge capacity and coulombic efficiency compared with the

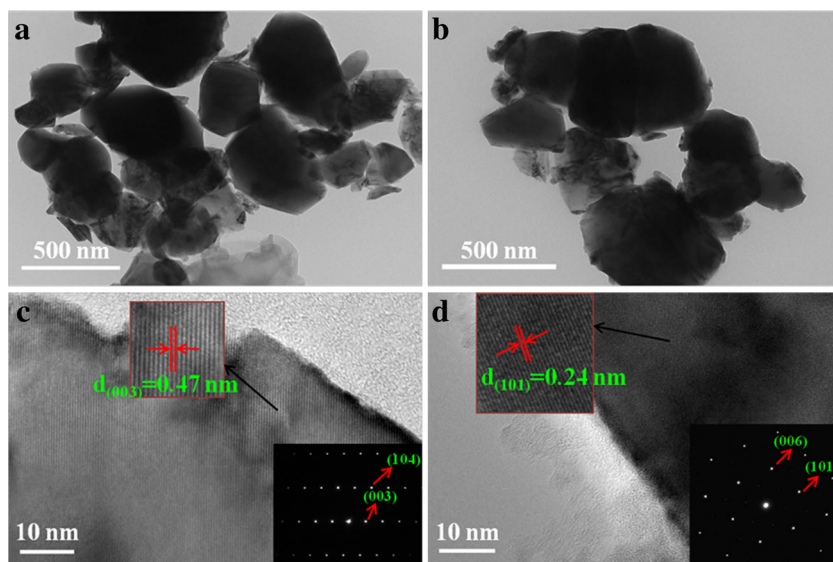
LMNC electrode. In addition, the high-level doping can sharply decrease the initial discharge capacity and coulombic efficiency of the Li-rich material.

Figure 6b exhibits the cycle performance of the LMNC and LMNCS electrodes for 50 cycles at 0.1 C. From Fig. 6b, the LMNCS1 electrode always exhibits the highest discharge capacities among all electrodes during cycling and delivers a discharge capacity of  $199.8 \text{ mAh g}^{-1}$  with capacity retention of 75.2% after 50 cycles. Although the LMNCS0.5 electrode presents similar discharge capacities to the LMNC electrode in the initial cycles, it gradually exhibits higher capacities than LMNC in the consequent cycles. The LMNCS0.5 electrode still keeps a reversible discharge capacity of  $182.4 \text{ mAh g}^{-1}$  with capacity retention of 72.5% after 50 cycles, while the LMNC electrode remains only 66.8% ( $168.1 \text{ mAh g}^{-1}$ ) of the initial discharge capacity. For the LMNCS1.5 and LMNCS2 electrodes, the initial discharge capacities are much less than the others, but their capacity retentions are quite high

**Table 2** The element composition of analysis for LMNC and LMNCS1 measured by ICP

Sample	Li	Mn	Ni	Co	Sn
LMNC	1.136	0.540	0.132	0.129	0
LMNCS1	1.222	0.530	0.136	0.139	0.011

**Fig. 4** TEM images of the **a** LMNC and **b** LMNCS1 samples; HRTEM images of the **c** LMNC and **d** LMNCS1 samples (the insets are the corresponding fast Fourier transform patterns)



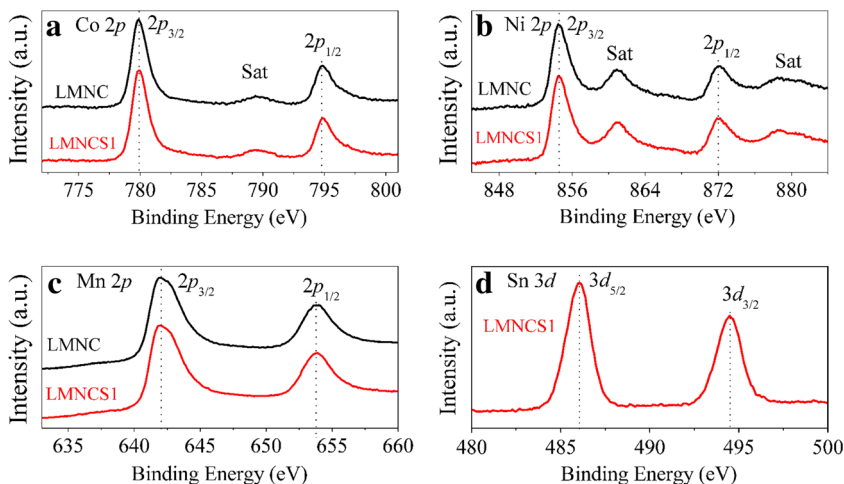
(95.1 and 81.0%, respectively). These results suggest that  $x = 0.01$  is the optimal doping amount of  $\text{Sn}^{4+}$  over the four Sn-doped samples to improve the specific capacity and cycle performance of the LMNC cathode. The Sn–O bond is stronger than Mn–O bond and the ionic radius of electrochemical inactive  $\text{Sn}^{4+}$  always stay unchanged during cycling, which can stabilize the framework of layered structure, leading to the enhancement of structural stability and cycling stability [38, 49].

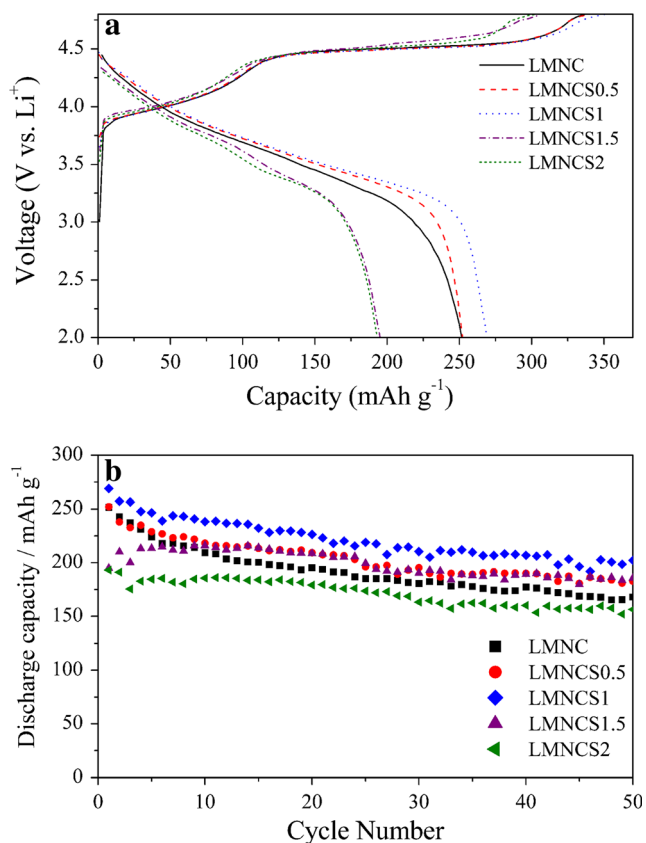
The charge/discharge curves of LMNC and LMNCS1 electrodes in the 1st, 10th, 20th, 30th, 40th, and 50th cycles at 0.1 C and the corresponding discharge midpoint potential of LMNC and LMNCS1 electrodes during 50 cycles are shown in Fig. 7. From Fig. 7a and b, the discharge capacities of LMNC and LMNCS1 continuously decrease during cycling. As marked by black arrows, the discharge profiles of both samples shift to the lower voltage plateau during cycling due to the increasing polarization. As we can see in Fig. 7c, the discharge midpoint potential for LMNC and LMNCS1 is similar in the initial 30

cycles, but the difference is more and more obvious in the further cycling. The discharge midpoint potential of LMNC reduces by 0.51 V ( $\Delta V$ ) after 50 cycles, while that of LMNCS1 exhibits a smaller  $\Delta V$  value (0.48 V). As the cycle number further increases, the difference of discharge midpoint potential for LMNC and LMNCS1 will become larger. This phenomenon has been frequently reported in recent investigations [41, 50–52]. This implies that the appropriate  $\text{Sn}^{4+}$ -doping could reduce the structural change of the LMNC material from the layered phase into the spinel phase during cycling [38]. As a result, the cycle performance of the LMNCS electrode is significantly enhanced.

Figure 8a shows the rate performance of the LMNC and LMNCS electrodes between 2.0 and 4.8 V, while Fig. 8b exhibits the variations of discharge capacities of the electrodes with discharge current density. From Fig. 8, the discharge capacities for all electrodes fade with the increasing discharge rate, which is attributed to the increased polarization at high rates [53]. The LMNCS0.5 and LMNCS1 electrodes exhibit

**Fig. 5** XPS spectra of **a** Co 2p, **b** Ni 2p, **c** Mn 2p, and **d** Sn 3d for the LMNC and LMNCS1 samples

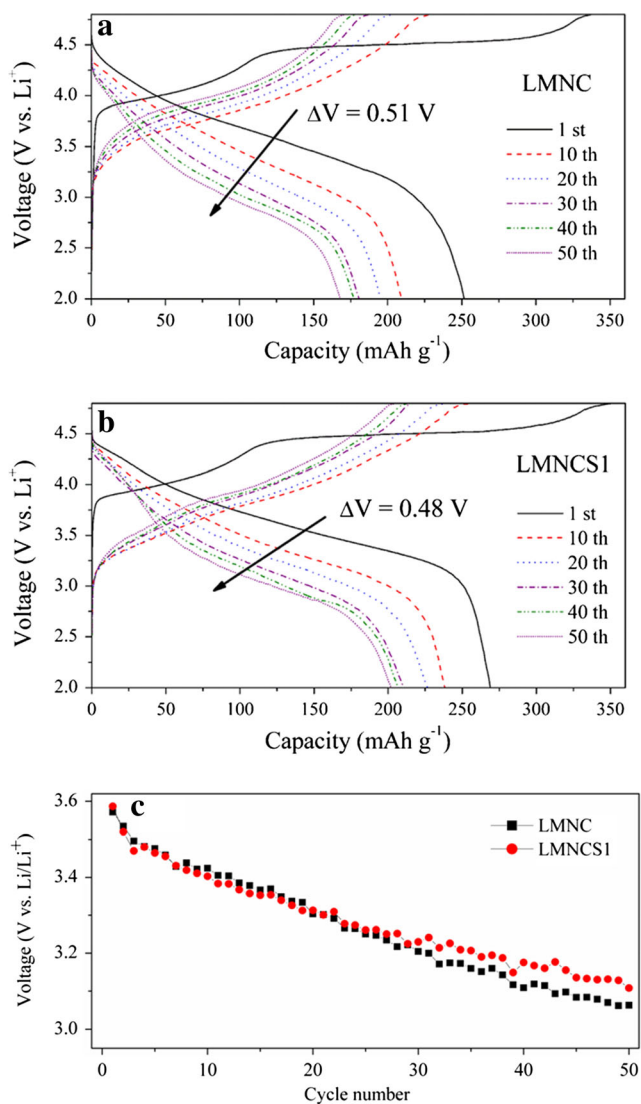




**Fig. 6** **a** Initial charge/discharge curves of the LMNC and LMNCS electrodes at 0.1 C between 2.0 and 4.8 V; **b** Cycling performance of the LMNC and LMNCS electrodes during 50 cycles at 0.1 C between 2.0 and 4.8 V

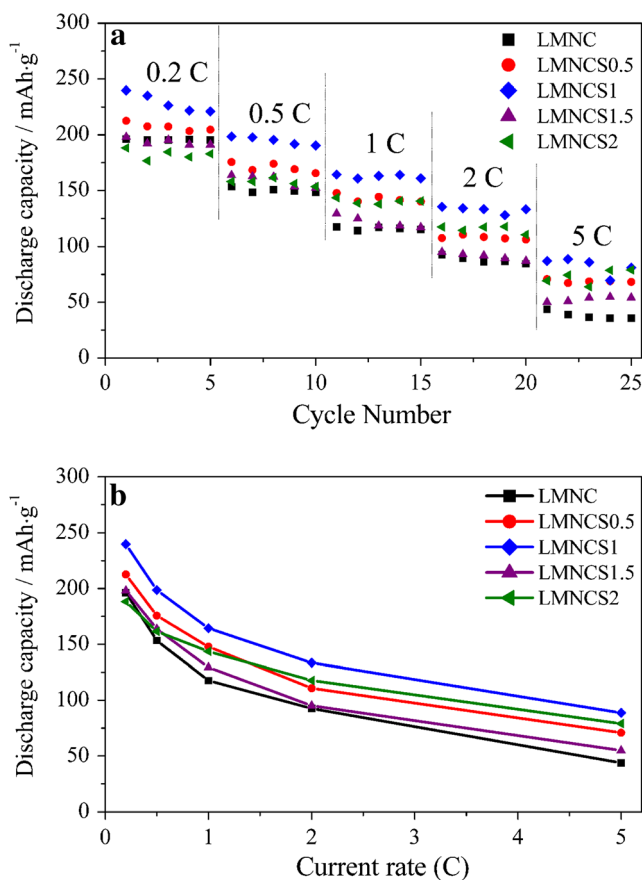
the significant enhanced rate capability when compared with the LMNC electrode. Although the LMNCS1.5 and LMNCS2 electrodes show similar discharge capacity to the LMNC electrode at low discharge rates, they deliver larger discharge capacity at high rates. Among all samples, the LMNCS1 cathode shows the optimal rate performance, giving the capacities of 239.8, 198.6, 164.4, 133.4, and 88.8 mAh g<sup>-1</sup> at 0.2, 0.5, 1, 2, and 5 C, respectively, which are superior to the LMNC cathode (196.2, 153.5, 117.5, 92.7, and 43.8 mAh g<sup>-1</sup> at 0.2, 0.5, 1, 2, and 5 C, respectively). Such prominent rate performance of the LMNCS electrodes is attributed to the enlargement of Li<sup>+</sup> diffusion channels caused by the doping of Sn<sup>4+</sup>, which is favorable to the intercalation/deintercalation of Li<sup>+</sup> [38, 49].

The CV curves of the LMNC and LMNCS1 cathodes in the initial five cycles are shown in Fig. 9. Both samples exhibit a characteristic CV curve of the Li-rich cathode materials [4, 24]. For the LMNC electrode (Fig. 9a), two oxidation peaks are observed in the initial charging curve, which are consistent with the two potential plateaus in the initial charge profile. The first one at ~4.1 V corresponds to the oxidation of TM ions (Ni<sup>2+</sup>/Co<sup>3+</sup> → Ni<sup>4+</sup>/Co<sup>4+</sup>), while another one at ~4.7 V is related to the irreversible removal of Li<sub>2</sub>O from Li<sub>2</sub>MnO<sub>3</sub>, which disappears in the subsequent cycles [5, 54]. In the



**Fig. 7** Charge/discharge curves of the **a** LMNC and **b** LMNCS1 electrodes in the 1st, 10th, 20th, 30th, 40th, and 50th cycles at 0.1 C between 2.0 and 4.8 V; **c** The corresponding discharge midpoint potential of LMNC and LMNCS1 samples during 50 cycles

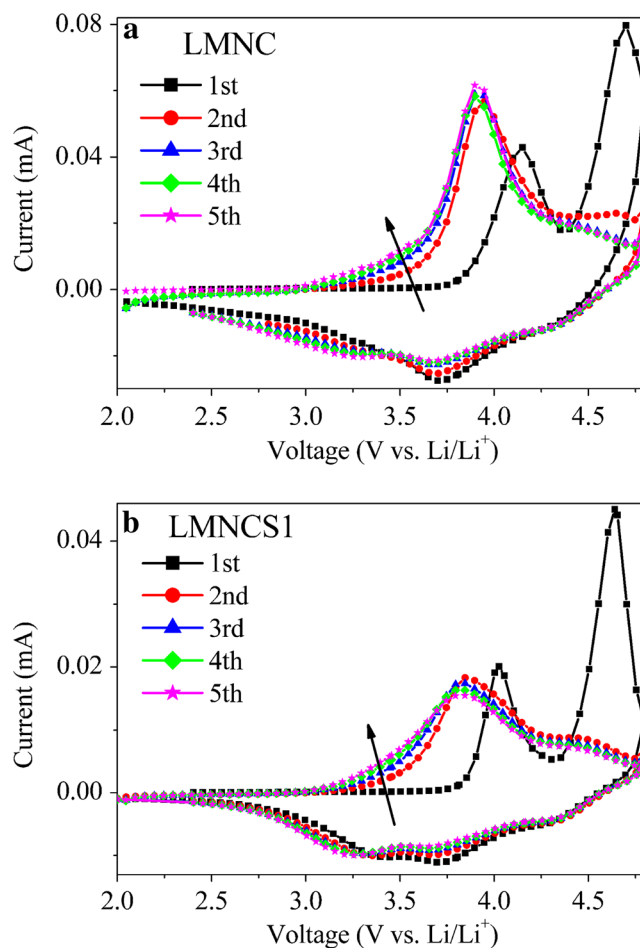
subsequent charging process, the first oxidation peak moves to left and locates at ~3.7 V. The 3.7 V oxidation peak for LMNC is sharper, while for LMNCS1, it is broader. This may be because the oxidation of Ni<sup>2+</sup> in LMNCS1 experiences multiple steps (Ni<sup>2+</sup> → Ni<sup>3+</sup> → Ni<sup>4+</sup>), while some of Ni<sup>2+</sup> is only oxidized to Ni<sup>3+</sup> in LMNC [55]. The evidence is shown in Fig. S1 and the length of charge stage for LMNCS1 in the 2nd, 3rd, 4th, and 5th cycles are all longer than that for LMNC. There are two reduction peaks at ~3.7 and 4.3 V in the initial discharging process, which are related to the reduction of Ni<sup>4+</sup> and Co<sup>4+</sup>, respectively [56, 57]. In the second discharging process, a new reduction peak occurs at ~3.25 V that involves the reduction of Mn ion (Mn<sup>4+</sup> → Mn<sup>3+</sup>) [58]. For the LMNCS1 electrode (Fig. 9b), the two oxidation peaks in the initial charging process are sharper and more



**Fig. 8** **a** Rate capability of the LMNC and LMNCS electrodes between 2.0 and 4.8 V; **b** Variations of the highest discharge capacity with discharge rate

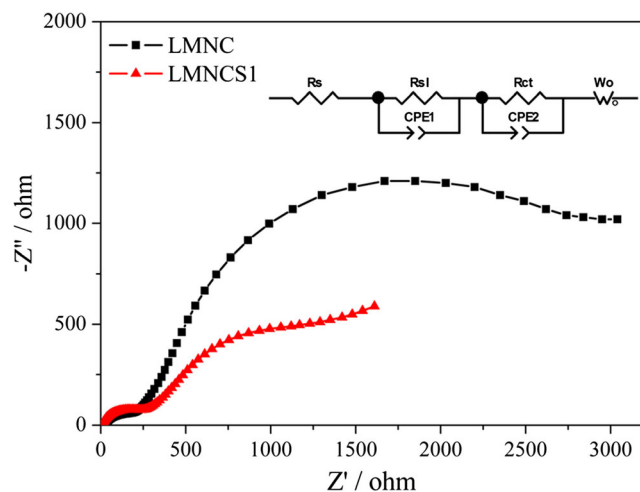
symmetrical than the LMNC. The cathodic peak at 3.25 V for LMNCS1 can be observed in the initial discharging process, indicating Mn is functionally activated, resulting in higher initial coulombic efficiency [58]. Moreover, the redox peaks of Ni<sup>2+</sup>/Ni<sup>4+</sup> redox couple for the LMNC and LMNCS1 electrodes are located at 3.72/4.14 and 3.71/4.02 V, respectively. Consequently, the peak potential difference of Ni<sup>2+</sup>/Ni<sup>4+</sup> redox couple for the LMNCS1 electrode is smaller (0.31 V) than that of the LMNC electrode (0.42 V). Furthermore, the CV curves of the LMNCS1 electrode are highly overlapped compared with that of LMNC. These results imply that the Sn<sup>4+</sup> doping can reduce the polarization of electrochemical redox and enhance the cyclic reversibility [59], which is in accordance with the enhancement of cycle stability.

Figure 10 shows the EIS spectra of the LMNC and LMNCS1 electrodes after 10 cycles. The Nyquist plots for these two cathode materials are made of three parts: two semicircles in a high-to-mid-frequency region and a tail in a low-frequency region. The two semicircles are assigned to the Li<sup>+</sup> diffusion through the surface layer and the charge transfer resistance in the interface of electrode/electrolyte, respectively, while the tail relates to the Li<sup>+</sup> diffusion process in the electrode materials. Table 3 exhibits the simulated electrochemical



**Fig. 9** Cycle voltammograms of the **a** LMNC and **b** LMNCS1 electrodes between 2.0 and 4.8 V, at a scan rate of 0.1 mV s<sup>-1</sup>

parameters from the Nyquist plots in Fig. 10, in which  $R_s$ ,  $R_{s1}$ ,  $R_{ct}$ , and  $D_{Li^+}$  are the internal resistance, the surface layer resistance, the charge transfer resistance of the cell, and the Li<sup>+</sup> diffusion coefficient, respectively. As shown in Table 3, the



**Fig. 10** Electrochemical impedance spectra of the LMNC and LMNCS1 electrodes after 10 cycles (The inset is the equivalent circuit for the impedance spectra)



**Table 3** Simulated data from EIS spectra of the LMNC and LMNCS1 electrodes after 10 cycles

Sample	$R_s$ ( $\Omega$ )	$R_{sl}$ ( $\Omega$ )	$R_{ct}$ ( $\Omega$ )	$D_{Li^+}$ ( $\text{cm}^2 \text{s}^{-1}$ )
LMNC	19.4	211.4	3662	$4.164 \times 10^{-14}$
LMNCS1	5.7	209.6	2315	$1.676 \times 10^{-13}$

values of  $R_s$  and  $R_{sl}$  for LMNCS1 are close to those for LMNC, while the value of  $R_{ct}$  for LMNCS1 is much smaller than that for LMNC. This indicates that the  $\text{Sn}^{4+}$ -doping can decrease the charge transfer resistance and improve the electrical conductivity of LMNC cathode material and thus enhance the cycle performance and rate capability [38]. The values of  $D_{Li^+}$  were calculated from the Nyquist plots using the following equation [59].

$$D_{Li^+} = \frac{0.5R^2T^2}{n^2F^4A^2C^2\sigma^2}$$

Herein,  $R$  is the gas constant,  $T$  is the absolute temperature,  $n$  is the number of the electrons in the reactions,  $F$  is the Faraday's constant,  $A$  is the area of the cathode,  $C$  is the concentration of  $\text{Li}^+$ , and  $\sigma$  is the Warburg factor which is related to  $Z'$ .

$$Z' = \sigma\omega^{-1/2}$$

where  $Z'$  is the real part of impedance and  $\omega$  is the angular frequency in the low-frequency region. The  $D_{Li^+}$  for LMNCS1 is  $1.67 \times 10^{-13} \text{ cm}^2 \text{ s}^{-1}$  that is much higher than that for LMNC ( $4.16 \times 10^{-14} \text{ cm}^2 \text{ s}^{-1}$ ), demonstrating that the appropriate  $\text{Sn}^{4+}$ -doping could facilitate the  $\text{Li}^+$  diffusion in electrodes.

## Conclusions

The  $\text{Sn}^{4+}$ -doped LMNC cathode materials with the enhanced electrochemical performance were synthesized using the sol-gel method. The electrochemical performance of  $\text{Sn}^{4+}$ -doped LMNC cathode has been significantly enhanced, especially when the doping amount of  $\text{Sn}^{4+}$  is 0.01. Compared to the pristine LMNC, the LMNCS1 electrode has higher initial discharge capacity ( $268.9 \text{ mAh g}^{-1}$  with the initial coulombic efficiency of 76.5%), better cycle stability ( $199.8 \text{ mAh g}^{-1}$  at 0.1 C with capacity retention of 75.2% after 100 cycles), and the superior rate capability ( $88.8 \text{ mAh g}^{-1}$  at 5 C). The XRD results indicate that all the samples are layered  $\alpha$ - $\text{NaFeO}_2$  structure without any impurity and the  $\text{Sn}^{4+}$ -doping ( $x = 0.005\text{--}0.02$ ) could expand the volume of unit cell. The CV curves and EIS measurement demonstrate that the  $\text{Sn}^{4+}$ -doping could alleviate the electrochemical polarization and increase the value of  $D_{Li^+}$ .

These suggest a faster  $\text{Li}^+$  diffusion process and better structural stability, which are favorable for the electrochemical performance of the LMNC cathode material.

**Acknowledgements** This work was supported by the national college students' innovation and entrepreneurship training program (201510636004), the outstanding graduate theses foundation of Sichuan Normal University (2016-4-32), and the large precision instrument projects of Sichuan Normal University (DJ2016-27).

## References

- Goodenough JB, Kim Y (2010) Challenges for rechargeable Li batteries. *Chem Mater* 22:587–603
- Etacheri V, Marom R, Elazari R, Salitra G, Aurbach D (2011) Challenges in the development of advanced Li-ion batteries: a review. *Energy Environ Sci* 4:3243–3262
- Wang Z, Luo S, Ren J, Wang D, Qi X (2016) Enhanced electrochemical performance of Li-rich cathode  $\text{Li}[\text{Li}_{0.2}\text{Mn}_{0.54}\text{Ni}_{0.13}\text{Co}_{0.13}]\text{O}_2$  by surface modification with lithium ion conductor  $\text{Li}_3\text{PO}_4$ . *Appl Surf Sci* 370:437–444
- Wang YX, Shang KH, He W, Ai XP, Cao YL, Yang HX (2015) Magnesium-doped  $\text{Li}_{1.2}[\text{Co}_{0.13}\text{Ni}_{0.13}\text{Mn}_{0.54}]\text{O}_2$  for lithium-ion battery cathode with enhanced cycling stability and rate capability. *ACS Appl Mater Interfaces* 7:13014–13021
- Thackeray MM, Kang SH, Johnson CS, Vaughey JT, Benedek R, Hackney SA (2007)  $\text{Li}_2\text{MnO}_3$ -stabilized  $\text{LiMO}_2$  (M= Mn, Ni, Co) electrodes for lithium-ion batteries. *J Mater Chem* 17:3112–3125
- Ito A, Li D, Ohsawa Y, Sato Y (2008) A new approach to improve the high-voltage cyclic performance of Li-rich layered cathode material by electrochemical pre-treatment. *J Power Sources* 183:344–346
- Thackeray MM, Johnson CS, Vaughey JT, Li N, Hackney SA (2005) Advances in manganese-oxide 'composite' electrodes for lithium-ion batteries. *J Mater Chem* 15:2257–2267
- Venkateswara Rao C, Soler J, Katiyar R, Shojan J, West WC, Katiyar RS (2014) Investigations on electrochemical behavior and structural stability of  $\text{Li}_{1.2}\text{Mn}_{0.54}\text{Ni}_{0.13}\text{Co}_{0.13}\text{O}_2$  lithium-ion cathodes via in-situ and ex-situ Raman spectroscopy. *J Phys Chem C* 118:14133–14141
- Guo XJ, Li YX, Zheng M, Zheng JM, Li J, Gong ZL, Yang Y (2008) Structural and electrochemical characterization of  $x\text{Li}[\text{Li}_{1/3}\text{Mn}_{2/3}]\text{O}_2 \cdot (1-x)\text{Li}[\text{Ni}_{1/3}\text{Mn}_{1/3}\text{Co}_{1/3}]\text{O}_2$  ( $0 \leq x \leq 0.9$ ) as cathode materials for lithium ion batteries. *J Power Sources* 184:414–419
- Lu H, Dahn JR (2002) Understanding the anomalous capacity of  $\text{Li}/\text{Li}[\text{Ni}_x\text{Li}_{(1/3-2x/3)}\text{Mn}_{(2/3-x/3)}]\text{O}_2$  cells using in situ X-ray diffraction and electrochemical studies. *J Electrochem Soc* 149:A815–A822
- Johnson CS, Kim JS, Lefief C, Li N, Vaughey JT, Thackeray MM (2004) The significance of the  $\text{Li}_2\text{MnO}_3$  component in 'composite'  $x\text{Li}_2\text{MnO}_3 \cdot (1-x)\text{LiMn}_{0.5}\text{Ni}_{0.5}\text{O}_2$  electrodes. *Electrochem Commun* 6:1085–1091
- Yu H, Wang Y, Asakura D, Hosono E, Zhang T, Zhou H (2012) Electrochemical kinetics of the  $0.5\text{Li}_2\text{MnO}_3 \cdot 0.5\text{LiMn}_{0.42}\text{Ni}_{0.42}\text{Co}_{0.16}\text{O}_2$  'composite' layered cathode material for lithium-ion batteries. *RSC Adv* 2:8797–8807
- Zhang HZ, Qiao QQ, Li GR, Ye SH, Gao XP (2012) Surface nitridation of Li-rich layered  $\text{Li}(\text{Li}_{0.17}\text{Ni}_{0.25}\text{Mn}_{0.58})\text{O}_2$  oxide as cathode material for lithium-ion battery. *J Mater Chem* 22:13104–13109
- Armstrong AR, Holzapfel M, Novák P, Johnson CS, Kang SH, Thackeray MM, Bruce PG (2006) Demonstrating oxygen loss

- and associated structural reorganization in the lithium battery cathode  $\text{Li}[\text{Ni}_{0.2}\text{Li}_{0.2}\text{Mn}_{0.6}]\text{O}_2$ . *J Am Chem Soc* 128:8694–8698
15. Kang SH, Kempgens P, Greenbaum S, Kropf AJ, Amine K, Thackeray MM (2007) Interpreting the structural and electrochemical complexity of  $0.5\text{Li}_2\text{MnO}_3 \cdot 0.5\text{LiMO}_2$  electrodes for lithium batteries ( $\text{M} = \text{Mn}_{0.5-x}\text{Ni}_{0.5-x}\text{Co}_{2x}$ ,  $0 \leq x \leq 0.5$ ). *J Mater Chem* 17: 2069–2077
  16. Johnson CS, Li N, Lefief C, Thackeray MM (2007) Anomalous capacity and cycling stability of  $x\text{Li}_2\text{MnO}_3 \cdot (1-x)\text{LiMO}_2$  electrodes ( $\text{M} = \text{Mn}, \text{Ni}, \text{Co}$ ) in lithium batteries at 50 °C. *Electrochem Commun* 9(4):787–795
  17. Manthiram A, Knight JC, Myung ST, Oh SM, Sun YK (2016) Nickel-rich and lithium-rich layered oxide cathodes: progress and perspectives. *Adv Energy Mater* 6:1501010
  18. Liu X, Huang T, Yu A (2015) Surface phase transformation and  $\text{CaF}_2$  coating for enhanced electrochemical performance of Li-rich Mn-based cathodes. *Electrochim Acta* 163:82–92
  19. Lu C, Wu H, Zhang Y, Liu H, Chen B, Wu N, Wang S (2014) Cerium fluoride coated layered oxide  $\text{Li}[\text{Li}_{0.2}\text{Mn}_{0.54}\text{Ni}_{0.13}\text{Co}_{0.13}]\text{O}_2$  as cathode materials with improved electrochemical performance for lithium ion batteries. *J Power Sources* 267:682–691
  20. Kang SH, Johnson CS, Vaughey JT, Amine K, Thackeray MM (2006) The effects of acid treatment on the electrochemical properties of  $0.5\text{Li}_2\text{MnO}_3 \cdot 0.5\text{LiNi}_{0.44}\text{Co}_{0.25}\text{Mn}_{0.31}\text{O}_2$  electrodes in lithium cells. *J Electrochem Soc* 153:A1186–A1192
  21. Kang SH, Thackeray MM (2008) Stabilization of  $x\text{Li}_2\text{MnO}_3 \cdot (1-x)\text{LiMO}_2$  electrode surfaces ( $\text{M} = \text{Mn}, \text{Ni}, \text{Co}$ ) with mildly acidic fluorinated solutions. *J Electrochem Soc* 155:A269–A275
  22. Wang D, Belharouak I, Ortega LH, Zhang X, Xu R, Zhou D, Zhou G, Amine K (2015) Synthesis of high capacity cathodes for lithium-ion batteries by morphology-tailored hydroxide co-precipitation. *J Power Sources* 274:451–457
  23. Fu F, Deng YP, Shen CH, Xu GL, Peng XX, Wang Q, Xu YF, Fang JC, Huang L, Sun SG (2014) A hierarchical micro/nanostructured  $0.5\text{Li}_2\text{MnO}_3 \cdot 0.5\text{LiMn}_{0.4}\text{Ni}_{0.3}\text{Co}_{0.3}\text{O}_2$  material synthesized by solvothermal route as high rate cathode of lithium ion battery. *Electrochem Commun* 44:54–58
  24. He W, Yuan D, Qian J, Ai X, Yang H, Cao Y (2013) Enhanced high-rate capability and cycling stability of Na-stabilized layered  $\text{Li}_{1.2}[\text{Co}_{0.13}\text{Ni}_{0.13}\text{Mn}_{0.54}]\text{O}_2$  cathode material. *J Mater Chem A* 1: 11397–11403
  25. Liu X, Liu J, Huang T, Yu A (2013)  $\text{CaF}_2$ -coated  $\text{Li}[\text{Li}_{0.2}\text{Mn}_{0.54}\text{Ni}_{0.13}\text{Co}_{0.13}]\text{O}_2$  as cathode materials for Li-ion batteries. *Electrochim. Acta* 109:52–58
  26. Li Q, Li G, Fu C, Luo D, Fan J, Li L (2014)  $\text{K}^+$ -doped  $\text{Li}_{1.2}\text{Mn}_{0.54}\text{Co}_{0.13}\text{Ni}_{0.13}\text{O}_2$ : a novel cathode material with an enhanced cycling stability for lithium-ion batteries. *ACS Appl Mater Interfaces* 6:10330–10341
  27. Wang D, Huang Y, Huo Z, Chen L (2013) Synthesize and electrochemical characterization of Mg-doped Li-rich layered  $\text{Li}[\text{Li}_{0.2}\text{Ni}_{0.2}\text{Mn}_{0.6}]\text{O}_2$  cathode material. *Electrochim. Acta* 107: 461–466
  28. Zhao J, Wang Z, Guo H, Li X, He Z, Li T (2015) Synthesis and electrochemical characterization of Zn-doped Li-rich layered  $\text{Li}[\text{Li}_{0.2}\text{Mn}_{0.54}\text{Ni}_{0.13}\text{Co}_{0.13}]\text{O}_2$  cathode material. *Ceram Int* 41(9): 11396–11401
  29. Zhang WH, He W, Pei F, Wu FY, Mao RJ, Ai XP, Yang HX, Cao YL (2013) Improved electrochemical properties of  $\text{Al}^{3+}$ -doped  $0.5\text{Li}_2\text{MnO}_3 \cdot 0.5\text{LiCo}_{1/3}\text{Ni}_{1/3}\text{Mn}_{1/3}\text{O}_2$  cathode for lithium ion batteries. *J Inorg Mater* 28:1261–1264
  30. Jiao LF, Zhang M, Yuan HT, Zhao M, Guo J, Wang W, Zhou XD, Wang YM (2007) Effect of Cr doping on the structural, electrochemical properties of  $\text{Li}[\text{Li}_{0.2}\text{Ni}_{0.2-x/2}\text{Mn}_{0.6-x/2}\text{Cr}_x]\text{O}_2$  ( $x = 0, 0.02, 0.04, 0.06, 0.08$ ) as cathode materials for lithium secondary batteries. *J Power Sources* 167:178–184
  31. Yan J, Liu X, Li B (2014) Recent progress in Li-rich layered oxides as cathode materials for Li-ion batteries. *RSC Adv* 4:63268–63284
  32. Song B, Lai MO, Lu L (2012) Influence of Ru substitution on Li-rich  $0.55\text{Li}_2\text{MnO}_3 \cdot 0.45\text{LiNi}_{1/3}\text{Co}_{1/3}\text{Mn}_{1/3}\text{O}_2$  cathode for Li-ion batteries. *Electrochim. Acta* 80:187–195
  33. Jin X, Xu Q, Liu H, Yuan X, Xia Y (2014) Excellent rate capability of Mg doped  $\text{Li}[\text{Li}_{0.2}\text{Ni}_{0.13}\text{Co}_{0.13}\text{Mn}_{0.54}]\text{O}_2$  cathode material for lithium-ion battery. *Electrochim Acta* 136:19–26
  34. He Z, Wang Z, Chen H, Huang Z, Li X, Guo H, Wang R (2015) Electrochemical performance of zirconium doped lithium rich layered  $\text{Li}_{1.2}\text{Mn}_{0.54}\text{Ni}_{0.13}\text{Co}_{0.13}\text{O}_2$  oxide with porous hollow structure. *J Power Sources* 299:334–341
  35. Xia Y, Shi S, Li C, Liang C, Gan Y, Huang H, Tao X, Zhang W (2015) Electrochemical properties of Sn-doped  $\text{Li}_3\text{V}_2(\text{PO}_4)_3$  cathode material synthesized via a citric acid assisted sol-gel method. *J Alloys Compd* 652:298–306
  36. Ma J, Li B, Du H, Xu C, Kang F (2011) Effects of tin doping on physicochemical and electrochemical performances of  $\text{LiFe}_{1-x}\text{Sn}_x\text{PO}_4/\text{C}$  ( $0 \leq x \leq 0.07$ ) composite cathode materials. *Electrochim. Acta* 56:7385–7391
  37. Ren H, Mu X, Huang Y, Li Z, Wang Y, Cai P, Peng Z, Zhou Y (2010) Effects of Sn doping on electrochemical characterizations of  $\text{Li}[\text{Ni}_{1/3}\text{Co}_{1/3}\text{Mn}_{1/3}]\text{O}_2$  cathode material. *Ionics* 16:497–502
  38. Zhao Y, Xia M, Hu X, Zhao Z, Wang Y, Lv Z (2015) Effects of Sn doping on the structural and electrochemical properties of  $\text{Li}_{1.2}\text{Ni}_{0.2}\text{Mn}_{0.8}\text{O}_2$  Li-rich cathode materials. *Electrochim. Acta* 174:1167–1174
  39. Zhou L, Tian M, Deng Y, Zheng Q, Xu C, Lin D (2016)  $\text{La}_2\text{O}_3$ -coated  $\text{Li}_{1.2}\text{Mn}_{0.54}\text{Ni}_{0.13}\text{Co}_{0.13}\text{O}_2$  as cathode materials with enhanced specific capacity and cycling stability for lithium-ion batteries. *Ceram Int* 42:15623–15633
  40. Zheng J, Wu X, Yang Y (2013) Improved electrochemical performance of  $\text{Li}[\text{Li}_{0.2}\text{Mn}_{0.54}\text{Ni}_{0.13}\text{Co}_{0.13}]\text{O}_2$  cathode material by fluorine incorporation. *Electrochim. Acta* 105:200–208
  41. Sun L, Yi X, Ren X, Zhang P, Liu J (2016) Synthesis and electrochemical performances of Y-doped lithium-rich layered  $\text{Li}[\text{Li}_{0.2}\text{Ni}_{0.2}\text{Mn}_{0.6}]\text{O}_2$  cathode material. *J Electrochem Soc* 163: A766–A772
  42. Han E, Li Y, Zhu L, Zhao L (2014) The effect of  $\text{MgO}$  coating on  $\text{Li}_{1.17}\text{Mn}_{0.48}\text{Ni}_{0.23}\text{Co}_{0.12}\text{O}_2$  cathode material for lithium ion batteries. *Solid State Ionics* 255:113–119
  43. Yuan W, Zhang HZ, Liu Q, Li GR, Gao XP (2014) Surface modification of  $\text{Li}(\text{Li}_{0.17}\text{Ni}_{0.2}\text{Co}_{0.05}\text{Mn}_{0.58})\text{O}_2$  with  $\text{CeO}_2$  as cathode material for Li-ion batteries. *Electrochim Acta* 135:199–207
  44. Zhang Y, Hou P, Zhou E, Shi X, Wang X, Song D, Guo J, Zhang L (2015) Pre-heat treatment of carbonate precursor firstly in nitrogen and then oxygen atmospheres: a new procedure to improve tap density of high-performance cathode material  $\text{Li}_{1.167}(\text{Ni}_{0.139}\text{Co}_{0.139}\text{Mn}_{0.556})\text{O}_2$  for lithium ion batteries. *J Power Sources* 292:58–65
  45. Ma D, Li Y, Zhang P, Cooper AJ, Abdelkader AM, Ren X, Deng L (2016) Mesoporous  $\text{Li}_{1.2}\text{Mn}_{0.54}\text{Ni}_{0.13}\text{Co}_{0.13}\text{O}_2$  nanotubes for high-performance cathodes in Li-ion batteries. *J Power Sources* 311:35–41
  46. Wang J, He X, Paillard E, Laszczynski N, Li J, Passerini S (2016) Lithium- and manganese-rich oxide cathode materials for high-energy lithium ion batteries. *Adv. Energy Mater* 6(21):1600906
  47. Shi SJ, Tu JP, Mai YJ, Zhang YQ, Gu CD, Wang XL (2012) Effect of carbon coating on electrochemical performance of  $\text{Li}_{1.048}\text{Mn}_{0.381}\text{Ni}_{0.286}\text{Co}_{0.286}\text{O}_2$  cathode material for lithium-ion batteries. *Electrochim Acta* 63:112–117
  48. Sun YY, Li F, Qiao QQ, Cao JS, Wang YL, Ye SH (2015) Surface modification of  $\text{Li}(\text{Li}_{0.17}\text{Ni}_{0.2}\text{Co}_{0.05}\text{Mn}_{0.58})\text{O}_2$  with  $\text{LiAlSiO}_4$  fast ion conductor as cathode material for Li-ion batteries. *Electrochim Acta* 176:1464–1475

49. Qiao QQ, Qin L, Li GR, Wang YL, Gao XP (2015) Sn-stabilized Li-rich layered  $\text{Li}(\text{Li}_{0.17}\text{Ni}_{0.25}\text{Mn}_{0.58})\text{O}_2$  oxide as a cathode for advanced lithium-ion batteries. *J Mater Chem A* 3:17627–17634
50. Lee E, Koritala R, Miller DJ, Johnson CS (2015) Aluminum and gallium substitution into  $0.5\text{Li}_2\text{MnO}_3 \cdot 0.5\text{Li}(\text{Ni}_{0.375}\text{Mn}_{0.375}\text{Co}_{0.25})\text{O}_2$  layered composite and the voltage fade effect. *J Electrochem Soc* 162(3):A322–A329
51. Feng X, Gao Y, Ben L, Yang Z, Wang Z, Chen L (2016) Enhanced electrochemical performance of Ti-doped  $\text{Li}_{1.2}\text{Mn}_{0.54}\text{Co}_{0.13}\text{Ni}_{0.13}\text{O}_2$  for lithium-ion batteries. *J Power Sources* 317:74–80
52. Zhang HZ, Li F, Pan GL, Li GR, Gao XP (2015) The effect of polyanion-doping on the structure and electrochemical performance of Li-rich layered oxides as cathode for lithium-ion batteries. *J Electrochem Soc* 162(9):A1899–A1904
53. Chen M, Chen D, Liao Y, Zhong X, Li W, Zhang Y (2016) Layered lithium-rich oxide nanoparticles doped with spinel phase: acidic sucrose-assisted synthesis and excellent performance as cathode of lithium ion battery. *ACS Appl Mater Interfaces* 8:4575–4584
54. Amalraj F, Talianker M, Markovsky B, Sharon D, Burlaka L, Shafir G, Zinigrad E, HaikO AD, Lampert J, Schulz-Dobrick M, Garsuch A (2013) Study of the lithium-rich integrated compound  $x\text{Li}_2\text{MnO}_3 \cdot (1-x)\text{LiMO}_2$  ( $x$  around 0.5;  $M = \text{Mn, Ni, Co}$ ; 2: 2: 1) and its electrochemical activity as positive electrode in lithium cells. *J Electrochem Soc* 160(2):A324–A337
55. Ates MN, Mukerjee S, Abraham KM (2014) A Li-rich layered cathode material with enhanced structural stability and rate capability for Li-ion batteries. *J Electrochem Soc* 161(3):A355–A363
56. Wang C, Zhou F, Chen K, Kong J, Jiang Y, Yan G, Li J, Yu C, Tang W (2015) Electrochemical properties of  $\alpha\text{-MoO}_3$ -coated  $\text{Li}[\text{Li}_{0.2}\text{Mn}_{0.54}\text{Ni}_{0.13}\text{Co}_{0.13}]\text{O}_2$  cathode material for Li-ion batteries. *Electrochim Acta* 176:1171–1181
57. He W, Qian J, Cao Y, Ai X, Yang H (2012) Improved electrochemical performances of nanocrystalline  $\text{Li}[\text{Li}_{0.2}\text{Mn}_{0.54}\text{Ni}_{0.13}\text{Co}_{0.13}]\text{O}_2$  cathode material for Li-ion batteries. *RSC Adv* 2(8):3423–3429
58. Li F, Sun YY, Yao ZH, Cao JS, Wang YL, Ye SH (2015) Enhanced initial coulombic efficiency of  $\text{Li}_{1.14}\text{Ni}_{0.16}\text{Co}_{0.08}\text{Mn}_{0.57}\text{O}_2$  cathode materials with superior performance for lithium-ion batteries. *Electrochim Acta* 182:723–732
59. Yang S, Huang G, Hu S, Hou X, Huang Y, Yue M, Lei G (2014) Improved electrochemical performance of the  $\text{Li}_{1.2}\text{Ni}_{0.13}\text{Co}_{0.13}\text{Mn}_{0.54}\text{O}_2$  wired by CNT networks for lithium-ion batteries. *Mater Lett* 118:8–11